JOURNAL OF SOLID STATE CHEMISTRY 86, 212–232 (1990)

Incommensurate Misfit Layer Compounds of the Type "MTS_3" (M = Sn, Pb, Bi, Rare Earth Elements; T = Nb, Ta): A Study by Means of Electron Microscopy

S. KUYPERS, J. VAN LANDUYT, AND S. AMELINCKX

University of Antwerp (RUCA), Groenenborgerlaan 171, B-2020 Antwerpen, Belgium

Received August 15, 1989; in revised form December 4, 1989

Incommensurate misfit layer structures of the type "MTS_3" (M = Sn, Pb, Bi, rare earth elements; T = Nb, Ta) were studied by means of electron diffraction and high resolution electron microscopy. It is demonstrated how the electron diffraction patterns along the zone perpendicular to the layer planes can be interpreted in terms of the misfit between the constituent layers. Diffraction evidence for orientation variants is presented; their occurrence is directly related to the degree of deformation of the corresponding sublattices. With the use of image calculations it is shown how high resolution images in the layer plane directly reveal the incommensurate misfit through the varying coincidence of the atom columns of the two substructures. The shift of successive layers as reported from X-ray diffraction is found not to occur systematically in all crystals but it can give rise to stacking disorder.

1. Introduction

A systematic study was undertaken of the structures and physical properties of compounds of the type "MTS_3" (M = Sn, Pb, Bi, rare earth elements; T = Nb, Ta) (*1–7*). A preliminary review was given in (*8*). X-ray diffraction experiments on single crystals (*1–4, 6, 7*) showed all compounds to be made up of two-atom-thick MS layers and three-atom-thick TS_2 layers periodically alternating along the c-axis. The MS layers have a deformed NaCl-type structure, M being in a distorted square pyramidal coordination with sulfur (Fig. 1a). The TS_2 layers have a nearly undeformed 2H-NbS_2 structure, T being in a trigonal prismatic coordination with sulfur (Fig. 1b). If both substructures are described in C-centered orthorhombic cells with parameters, a_1, b_1, c_1 and a_2, b_2, c_2 for MS and TS_2, respectively, the corresponding axes are parallel. In the layer plane the (a_1, b_1) mesh and the (a_2, b_2) mesh fit along the b-direction ($b_1 = b_2$). Along all other directions in this plane there is an incommensurate misfit which is expressed by the ratio a_1/a_2 (Fig. 2). Due to the misfit the exact composition is $(MS)_nTS_2$, with $n = 2\ (a_2/a_1)$, rather than MTS_3. For most compounds a doubling of the c-parameter for the TS_2 part or for both the MS and the TS_2 parts is found from X-ray diffraction (*2, 3, 6–8*). It results from shifts over $b/2$ of subsequent layers of the same type leading to a face-centered unit cell for the substructure concerned. In Table I structural data (including the exact composition and the a_1/a_2 ratio) for the

0022-4596/90 $3.00

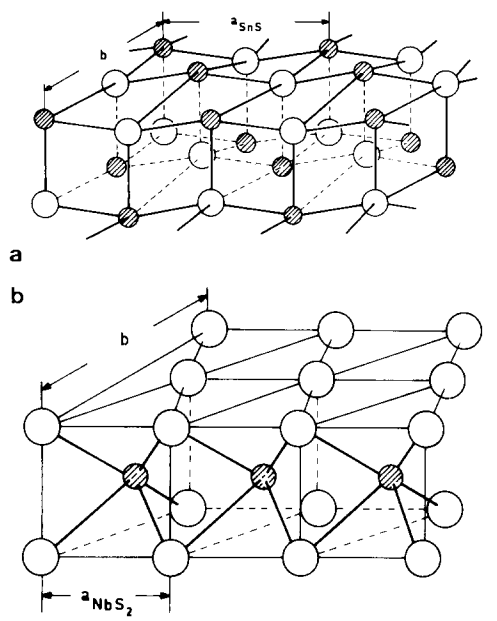

FIG. 1. (a) Slab of MS as present in the "MTS_3" compounds: the M atoms (striped spheres) slightly protrude and thus form the outer layers. (b) Slab of TS_2; the T atoms are in trigonal prismatic coordination by sulphur (open spheres). The a- and b-parameters of the orthorhombic unit meshes are given in Table I.

materials discussed in this paper are listed.

The compounds under study belong to the class of "noncommensurate misfit layer structures" (review in (*9*)). They are structurally closely related to the "$LaCrS_3$" family, members of which were studied earlier by various techniques including electron microscopy (*10, 11*). Other examples of misfit layer structures are found among the sulfosalts of which electron microscopic investigations were recently reported (*12, 13*).

2. Structural Considerations and Stacking Disorder

2.1 Disorder along the a-Direction

The structure of the MTS_3 compounds as determined from X-ray diffraction is obviously an average structure which may deviate locally from the actual structure. The structures of the MS and TS_2 lamellae were first determined separately using noncommon reflections and subsequently their relative positions were found from the common reflections (*4, 6, 7*). The resulting model thus consists of the unrelaxed superposition of lamellae of two perfectly periodic structures with different unit cells and different symmetries. The building principle is obvious from the projection along [001] of the structure model, shown in Fig. 2. The close-packed sulfur layers limiting the TS_2 lamellae offer zig-zag-shaped "grooves" or "furrows" along the close-packed directions. The average separation of these grooves is exactly the same as that of the atom rows in the MS layer, allowing perfect fit along the b-direction perpendicular to the grooves. The M and S atoms in the adjacent MS lamellae tend to occupy the triangular hollows formed by the sulfur atoms in the limiting layers of the TS_2 lamellae. Due to the difference in geometry of the two types of lamellae this is only possible for a limited number of M and S atoms. Hence the positioning of an MS lamella onto the sulfur layer of a TS_2 lamella has some degree of freedom. Small arbitrary shifts along the misfit direction presumably

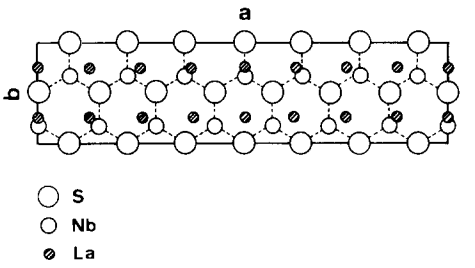

FIG. 2. Projection along [001] clearly revealing the misfit of MS and TS_2 along the a-direction in $(LaS)_{1.14}NbS_2$, "$LaNbS_3$." The ratio a_1/a_2 was approximated by 7/4 but is in fact irrational (Table I). The relative shifts over $b/2$ of successive NbS_2 layers as found from X-ray diffraction is not represented.

TABLE I

THE LATTICE PARAMETERS OF THE TWO STRUCTURAL UNITS (SU) OF THE DIFFERENT COMPOUNDS AS DERIVED FROM X-RAY DIFFRACTION (*8*) AND THE VALUE $2/\Delta g_1$ ($\approx na_1 \approx ma_2$) (IN Å)

Compound	SU	a	b	c	Stack	δ_1/δ_2	a_1/a_2	$2/\Delta g_1$	n, m
$(SnS)_{1.17}NbS_2$	SnS	5.673	5.751	11.76	TOTO	68	1.708	19.44	3.5
	NbS_2	3.321	5.751	11.76					6
$(SnS)_{1.15}TaS_2$	SnS	5.739	5.715	11.86	TOTO	1.2	1.733	21.52	3.5
	TaS_2	3.311	5.715	11.86					6
$(PbS)_{1.14}NbS_2$	PbS	5.832	5.801	11.90	TOTO'	.49	1.760	24.34	4
	NbS_2	3.313	5.801	23.80					7
$(PbS)_{1.14}TaS_2$	PbS	5.803	5.772	24.00	TOT'O'	.68	1.755	23.72	4
	TaS_2	3.306	5.772	24.00					7
$(LaS)_{1.14}NbS_2$	LaS	5.828	5.797	11.51	TOTO'	.49	1.761	24.36	4
	NbS_2	3.310	5.797	23.04					7
$(CeS)_{1.16}NbS_2$	CeS	5.728	5.767	11.41	TOTO'	1.10	1.731	21.30	3.5
	NbS_2	3.309	5.767	22.81					6
$(CeS)_{1.14}TaS_2$	CeS	5.737	5.749	11.44	TOTO'	.25	1.742	22.26	4
	TaS_2	3.293	5.752	22.89					7
$(SmS)_{1.18}TaS_2$	SmS	5.562	5.648	22.56	TOT'O'	1.61	1.690	17.92	3
	TaS_2	3.292	5.648	22.56					5
$(BiS)_{1.08}TaS_2$	BiS	6.101	5.738	23.13	TOT'O'	19	1.848	40.06	6.5
	TaS_2	3.302	5.738	23.13					12

Note. In the stacking sequence T and O represent MS and TS_2 slabs, respectively. (') indicates a relative shift over $b/2$. δ_1/δ_2 is the ratio of the relative deformations of the MS and TS_2 sublattices.

change very little the free energy associated with such a stacking (cf. phason modes). In different sandwiches the superposition patterns might thus have different "phases," leading to a particular type of disorder.

However, the absence of correlation between successive layers is contradicted by experiment, in particular by the sharp dots observed in high resolution images along the zone perpendicular to the layer planes. Even when a sideways shift along a occurs the correlation is apparently maintained (section 4.1). It is believed that elastic forces may contribute significantly to the correlation along the a-direction in the following way:

Successive lamellae will superpose in such a way that atoms occupy as much as possible the hollows in the neighboring layers. Therefore, "good" fit between lamellae can locally be achieved by minor changes in the interatomic distances along a; in one row the atoms will have to come closer together whereas in the next row their separation will slightly increase, i.e., one row will be under a "compressive" stress while the next is under a "tensile" stress. In Fig. 3 the situation before (a) and after (b) relaxation has been schematically represented. The arrows indicate the sense of the strain. A minimum in total strain energy will result if the regions of compressive stress overlap to the largest possible extent the regions of tensile stress. Due to the fact that both the MS and the TS_2 lamellae have a centered unit mesh the pattern of the sites of good fit will be centered as well, i.e., the stress pattern in successive a-rows along the b-direction will be reversed.

2.2 Translational Disorder

X-ray diffraction studies have revealed the occurrence in most of the compounds under study of discrete relative shifts over

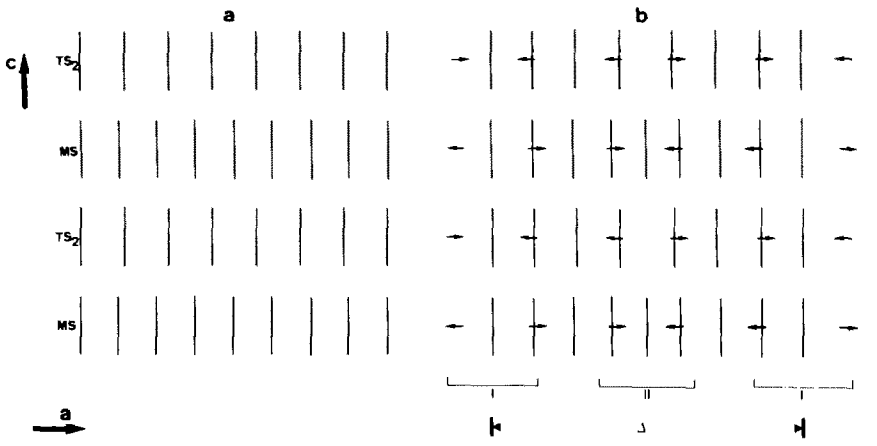

FIG. 3. Simplified model for the stress relaxation mechanism possibly responsible for the correlation along a between layers of the same type. The vertical lines represent atom columns in the respective lamellae.

$b/2$ of successive layers of the same type (*8*). As will be explained hereafter such displacements are readily understandable from the geometry of the structure. Note that both the limiting sulfur layers of a TS_2 lamella give rise to identical lattices of hollows which can be occupied by atoms of the MS lamellae. The vector $R_2 = 1/2\ [110]_2$ (Fig. 4a) is a "lattice" vector for the TS_2 structure but not for the MS structure. The following relation holds,

$$R_2 = 1/2\ [110]_2 = 1/4[1 + \varepsilon, 2, 0]_1,$$

where the subscript "1" refers to the MS lattice and "2" refers to the TS_2 lattice.

MS layers deposited on both sides of the same TS_2 reference layer can thus occupy with equal probability two different relative positions. They can either be stacked exactly vertical one above the other or their projected positions can differ by a displacement R_2 (Fig. 4a). Since arbitrary shifts along the misfit a-direction presumably occur very easily it is expected that the two MS lamellae on either side of the TS_2 lamella will rearrange slightly so as to adopt a stacking which is compatible with the minimization of the strain energy as discussed above. A small shift along a will allow the elimination of the component of the displacement vector along this direction (Fig. 4b). As a result two successive MS layers in the reference unit cell will either be stacked vertically above one another or they will be displaced one relative to the other over $1/2\ [010]_1 = 1/2\ [010]_2$.

Likewise $1/2\ [110]_1$ is a lattice vector for the MS structure but not for the TS_2 structure, the relation being

$$R_1 = 1/2\ [110]_1 = 1/2\ [2(1 - \varepsilon), 1, 0]_2.$$

Now the TS_2 lamellae on either side of an MS lamella will either come vertically above one another or they may be shifted over a displacement vector R_1 (Fig. 4c). The component of R_1 along a will presumably again be eliminated by a relative shift of the two TS_2 lamellae along this direction (Fig. 4d). As a result the two successive TS_2 layers either come vertically one above the other or are shifted over $1/2\ [010]$.

One thus obtains four essentially different basic stacking possibilities for a reference unit mesh:

(1) $T\ O\ T\ O$

(2) $T\ O\ T\ O'$

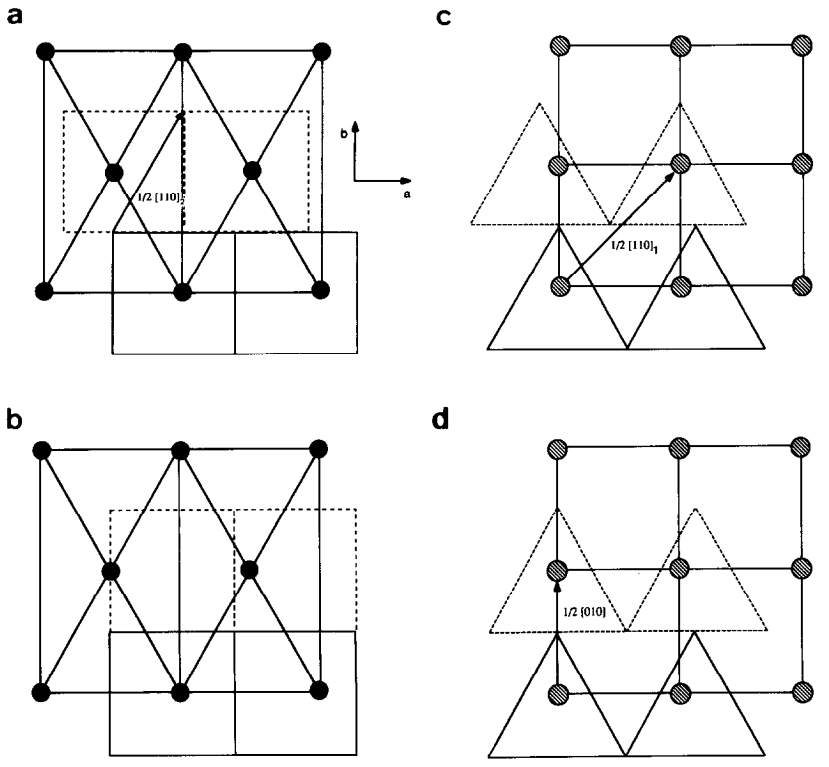

FIG. 4. Model explaining the presence of $b/2$ shifts between successive layers of MS or TS_2. (a) Two layers (represented by solid and broken lines, respectively) of MS on each side of a TS_2 slab are displaced over a "lattice" vector R_2 of TS_2. (b) A small relative shift of the MS layers along a results in a net displacement vector of 1/2 [010]. (c) Two layers (represented by solid and broken lines, respectively) of TS_2 on each side of an MS slab are displaced over a "lattice" vector R_1 of MS. (d) A small relative shift of the TS_2 layers along a results in a net displacement vector of 1/2 [010].

(3) $T\ O\ T'\ O$
(4) $T\ O\ T'\ O'$,
where T, T' and O, O' represent lamellae of MS ("tetragonal") and TS_2 ("orthohexagonal"), respectively; T and T' are related by a shift over 1/2 [010] as are O and O'. The different possibilities give rise to different c-parameters for the two substructures:
(1) $c_1 = c_2 \approx 1.2$ nm
(2) $c_1 \approx 1.2$ nm; $c_2 = 2c_1 \approx 2.4$ nm
(3) $c_2 \approx 1.2$ nm; $c_1 = 2c_2 \approx 2.4$ nm
(4) $c_1 = c_2 \approx 2.4$ nm.

The cases (1), (2), and (4) were actually found by X-ray diffraction experiments. The possibility of having two translation variants for each of the structures leads to the possibility of polytypism and of disordered structures. In the latter case the fault vector will always be 1/2 [010] irrespective of the reference structure. It is important to note that although 1/2 [010] is not a lattice vector of the MS structure a translation over this vector does not perturb the "square" configuration of atom columns in this substructure; however, a shift over 1/2 [010] does perturb the atom column configuration in the TS_2 part.

2.3 Orientational Disorder and Polytypism

On an undeformed MS layer with fourfold symmetry it is possible to deposit a TS_2 layer with pseudohexagonal (orthorhombic) symmetry, obeying the established epitaxial relationship, in two directions differ-

ing 90° in orientation. On the other hand on an undeformed TS_2 layer with hexagonal symmetry it is possible to deposit with equal probability an MS layer with pseudo-tetragonal (orthorhombic) symmetry in three orientations differing by 60°. Whether one or the other will happen depends on the degree of deformation of the two lattices on juxtaposition, as could be confirmed by our observations (Section 3.3).

If the hexagonal TS_2 lattice is the less deformed one, the three families of grooves in the close packed sulfur layers are almost equivalent and the disorder will preferentially occur in the MS layers. This can be understood as follows. An MS layer has in fact orthorhombic symmetry and one system of grooves in the NaCl-like arrangement will be preferred over the other. The next TS_2 layer will thus experience a bias to fit along the same family of grooves of the MS layer as the previous one. A rotation over 90° between successive TS_2 layers is then unlikely and as a result the correlation between the orientations of the two layers is rather strong. Whereas an MS layer has a choice between three almost equally favored possibilities the next TS_2 layer has no choice: the coincidence direction will be the same as that of the previous TS_2 layer.

If on the contrary the MS layer is the less deformed one, the two families of "grooves" in the MS layer are equivalent and therefore the orientational disorder will mainly occur in the TS_2 layers. The orthorhombic deformation of the TS_2 layer causes one family of grooves in this layer to become singular while the two others remain equivalent. Since the epitaxial fit occurs along the singular directions it is to be expected that the orientations of successive MS layers will now be highly correlated, whereas the TS_2 layers have a choice between two equally favored directions differing 90° (or 30°) in orientation.

One can imagine the orientational faults described here to occur in a periodic way and hence give rise to the formation of polytypes. Some evidence for this was indeed found in $PbNbS_3$ as will be shown in Section 3.3.

3. Electron Diffraction Observations

3.1 Sample Preparation

Single crystals of the different materials were prepared by vapor transport using chlorine as a transport agent; see, for example Refs. (*6–8*). The platelet shape of the crystals reflects the layered nature of the structures. Samples suitable for (high resolution) electron microscopy were prepared by repeated cleavage of the crystal platelets with adhesive tape. This technique naturally limits observations to directions close to the zone axis perpendicular to the layer planes, i.e., the [001] zone. Observations along zone axes in the layer plane were possible at curled up edges of thin foils or in samples obtained by cutting embedded platelets perpendicular to the layer planes with an ultramicrotome. However, the use of the latter technique was limited since it easily introduced severe deformations. Furthermore, the edge of a thin foil is always curled up in such a way that the axis of the "cylinder" is the b-direction, limiting observations to the [100] zone. This is understandable from the fact that elastic stresses associated with bending of the foil can most easily be released by small atom displacements along the misfit direction.

3.2 The [001] Zone

Electron diffraction patterns along the [001] zone, i.e., perpendicular to the layer planes, contain two sets of sharp "basic" spots due to the two sublattices, as well as sequences of extra spots perpendicular to the common diffraction vector (b^*) due to multiple diffraction and to the mutual modulation of the MS and TS_2 lamellae (Fig. 5) (*5*). A description of the symmetry of the complete structure and of the modulated substructures can be obtained by applica-

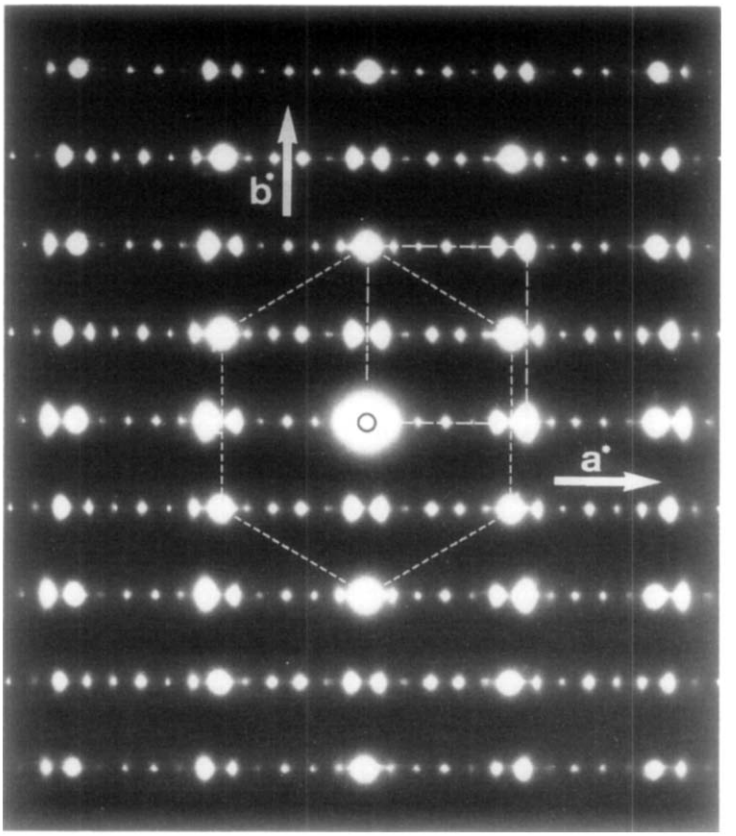

FIG. 5. Characteristic electron diffraction pattern along the [001] zone axis in an "MTS_3" compound ("$BiTaS_3$"). The pseudohexagonal and the nearly square configurations of intense spots are due to TS_2 (TaS_2) and MS (BiS), respectively. The extra spots are due to the complete structure.

tion of the theory of superspace groups (*14, 15*). In X-ray diffractograms the "satellite" spots are generally too weak to be observed and they were only reported in the case of $LaNbS_3$ (*3, 6*). The extra spots directly reveal the incommensurate misfit between the MS lattice and the TS_2 lattice and their positions can be derived from the basic spot positions by the difference vectors Δg_1, Δg_2, Δg_3 (Fig. 6), where $\Delta g_1 = \Delta g_2 + \Delta g_3$ and $|\Delta g_1| = (4/a_1) - (2/a_2)$.

The diffraction patterns can be interpreted as being composed of linear sequences of satellite spots associated with the MS spots in such a way that their spacing is Δg_1 and that they have fractional shifts of 1/2 with respect to the $hk0$ spots with $h + k =$ odd and no fractional shifts if $h + k =$ even. The TS_2 spots acquire the same sequence of satellites without fractional shifts, however. This is shown schematically in Fig. 6. The geometry of these patterns is consistent with a centered rectangular unit mesh for the coincidence structure with parameters $(2/\Delta g_1) \times b$; this is clearly only an approximation since in general $2/\Delta g_1$ is not a common multiple of spacings of MS and TS_2 (Table I). In Fig. 2 it was assumed that $7a_2 = 4a_1 = 2/\Delta g_1$.

The relative intensities of the spots due to MS and TS_2 were found to vary considerably from foil to foil and even within one

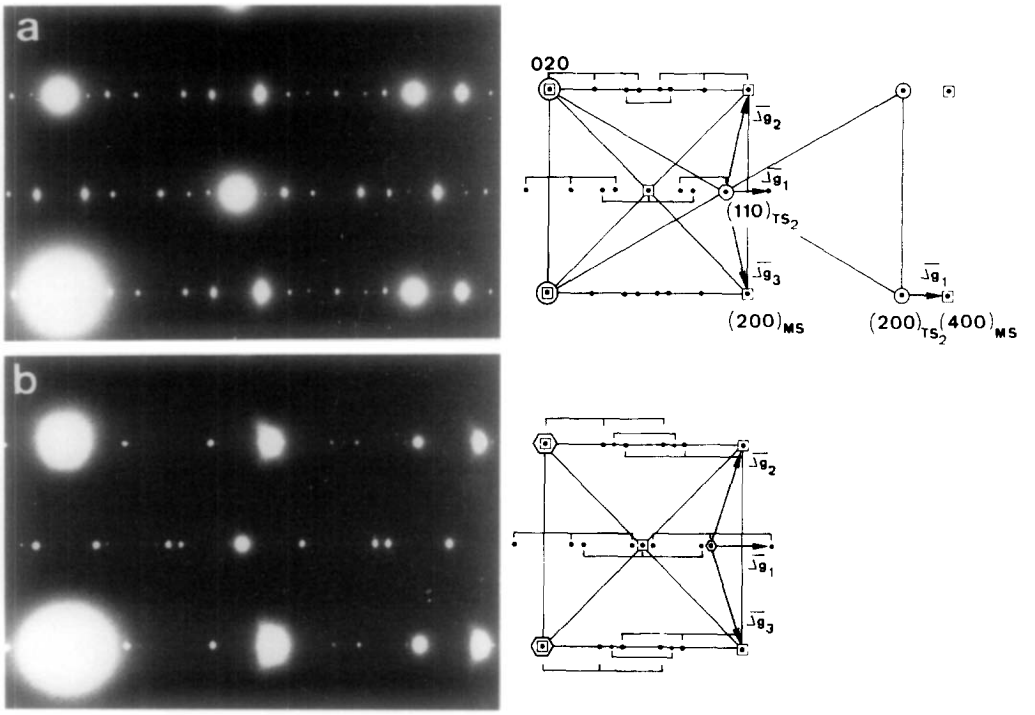

FIG. 6. Detail of electron diffraction patterns along the [001] zone axis of (a) $(PbS)_{1.14}NbS_2$, $a_2^*/a_1^* \approx 7/4$; (b) $(SnS)_{1.17}NbS_2$, $a_2^*/a_1^* \approx 12/7$. In the schematic representation on the right it is shown how the satellites can be generated from the basic spots by the difference vectors Δg_1, Δg_2, and Δg_3.

foil (compare, for example, Figs. 6a and 15). These variations are largely due to thickness variations as can be seen from Fig. 8 where the intensities of the 200_T reflection (due to MS) and the 100_O reflection (due to TS_2), calculated using the dynamical theory for electron diffraction, were plotted as a function of the foil thickness t. Generally one can state that in the first half of the experimental thickness range ($1.2 < t < 12$ nm) the "square" configuration of spots due to MS dominates, while in the second half ($12 < t < 24$ nm) the "hexagonal" configuration of spots due to TS_2 dominates.

One might expect the presence of an odd number of layers, i.e., the presence of an extra layer of one type, to also have a major influence on the relative intensities. However, the calculations show that one "excess" layer of MS or TS_2 only results in a relatively weak change of the intensities (Fig. 8b) and thus the experimental diffraction pattern will not be visibly influenced.

Although the [001] diffraction patterns of the different compounds have many features in common there are also characteristic differences. Some of the satellite patterns are commensurate within experimental error while others are visibly incommensurate. The diffraction patterns of several compounds have been represented in Figs. 5–7.

3.3 Orientational Variants

Regularly more intricate [001] zone patterns were observed in several of the com-

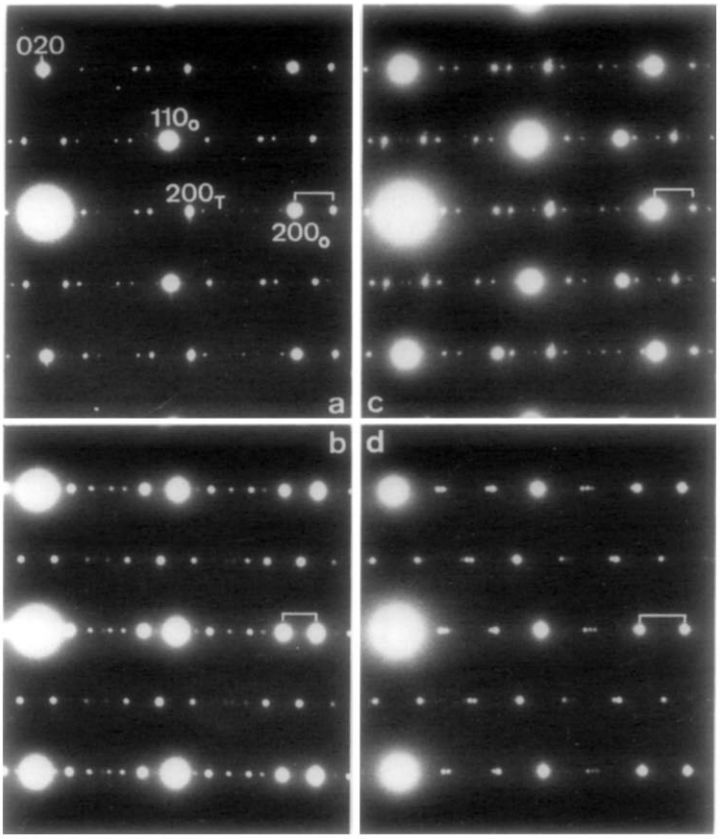

FIG. 7. Electron diffraction patterns along the [001] zone axis of different compounds. The configuration of satellite spots along a^* reflects the incommensurate ratio a_1/a_2 for each material (see Table I). (a) $(SnS)_{1.15}TaS_2$; (b) $(PbS)_{1.14}TaS_2$; (c) $(CeS)_{1.16}NbS_2$; (d) $(SmS)_{1.18}TaS_2$.

pounds (Figs. 9 and 10). They are due to different orientational variants of MS on TS_2 or vice versa. It was already suggested in section 2.3 that the variants that can occur for a specific compound can be predicted from the relative degree of deformation of the sublattices as measured from a "simple" [001] pattern or as deduced from the X-ray diffraction data (*8*) reproduced in Table I. The deformation of the centered tetragonal mesh was quantified as $\delta_1 = |a_1 - b_1|/b_1$ whereas the deformation of the orthohexagonal mesh was characterized by the expression $\delta_2 = |(a_2\sqrt{3}) - b_2|/b_2$.

From the values δ_1/δ_2 for the relative deformations (Table I) one expects:

—orientational variants of TS_2 in $PbNbS_3$, $PbTaS_3$, $LaNbS_3$, $CeTaS_3$;

—orientational variants of MS in $SnNbS_3$, $SmTaS_3$, $BiTaS_3$;

—both MS and TS_2 variants in $SnTaS_3$, $CeNbS_3$.

Electron diffraction patterns containing the expected variants and no others were indeed found, except for $PbTaS_3$ and $CeNbS_3$, in which no variants were observed as yet.

We shall discuss in some detail the diffraction pattern of Fig. 10a which refers to

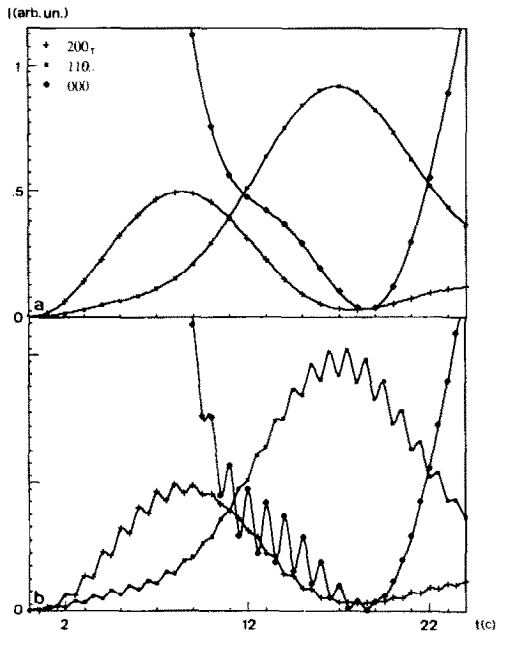

FIG. 8. Plot of calculated dynamical intensity I (in arbitr. units) versus foil thickness t (in c-units; c = 1.176 nm) for the reflections 000, 200_T, and 110_O of $SnNbS_3$; (a) t increases with $1c$, i.e., always an equal number of layers of each type is present; (b) t increases with (1/2) c illustrating in this way the effect of an extra layer of one type (here; NbS_2) on the diffracted intensity.

$PbNbS_3$ and is due to a stacking of MS double layers, all having the same orientation, interleaved with layers of TS_2 in such a way that successive TS_2 layers differ 30° (or 90°) in orientation. The "simple" diffraction pattern due to $PbNbS_3$ is shown in Fig. 6a. It exhibits the characteristic superposition of a square pattern due to the PbS layers and a hexagonal pattern due to the NbS_2 layers, as well as sequences of satellites oriented along the direction perpendicular to the common diffraction vector. From this pattern we can deduce the degree of deformation of the two lattices as a consequence of their superposition. Using the expressions for δ_1 and δ_2 given above one finds for the relative deformation of the sublattices $\delta_1/\delta_2 \approx 0.5$; i.e., the hexagonal lattice is the more deformed one. Following the considerations of Section 2.3 we can understand that the orientations of the MS layers are highly correlated, whereas the TS_2 layers can occur in two possible orientations which alternate along the c-direction. Since in the described structure the hexagonal layers occur in two mutually perpendicular orientations also the modulation satellite sequences occur in mutually perpendicular

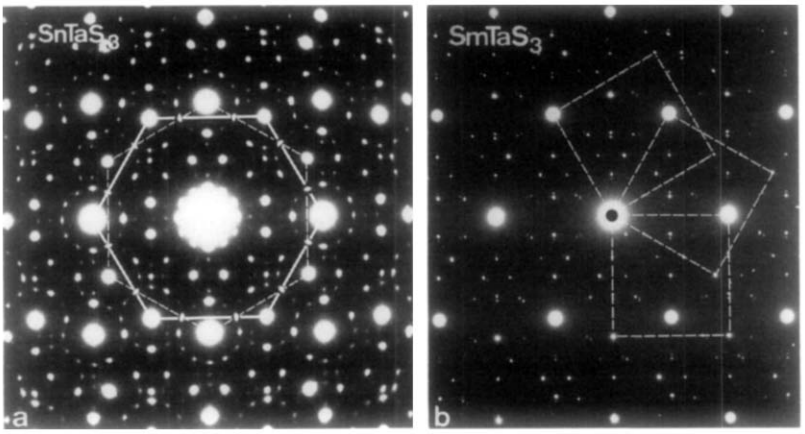

FIG. 9. Examples of more intricate [001] patterns due to the presence of orientational variants of the most deformed substructure: (a) in $SnTaS_3$; two variants of TaS_2 differing by 90° (30°), one variant of SnS; (b) in $SmTaS_3$; one variant of TaS_2, three variants of SmS differing by 60°.

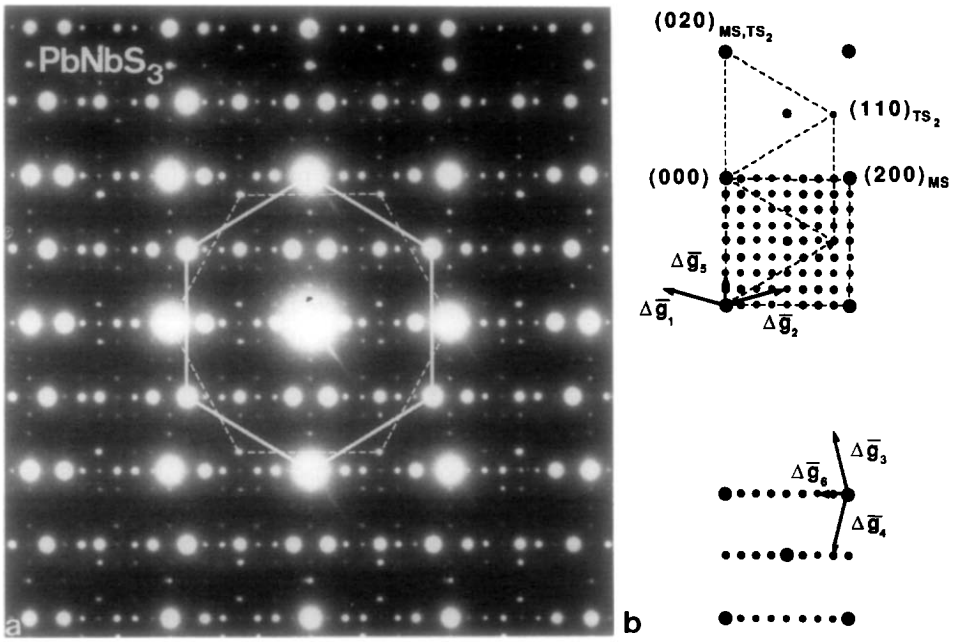

FIG. 10. Electron diffraction pattern along [001] in $PbNbS_3$ most likely due to a polytype consisting of an alternation of two variants of NbS_2 differing by 90° (30°) and one variant of PbS. The schematic representation on the right shows how all satellite reflections can be generated by the difference vectors Δg_i; $i = 1, 6$.

directions. The fact that a "filled-in" square grid is observed implies that multiple diffraction must occur between successive NbS_2 layers and therefore suggests that several NbS_2 layers superpose and contribute to the diffraction effects. The distances between the spots due to the square lattice are very nearly divided in eight equal intervals along both directions, suggesting the occurrence of an 8 × 8 superlattice for the composite structure. The square superlattice of satellite spots can in fact be generated from the *MS* lattice by the difference vectors Δg_1, Δg_2, Δg_3, Δg_4, Δg_5, and Δg_6 as represented in Fig. 10b.

3.4 The [100] Zone

In [100] zone patterns one generally observes that the spot rows 00*l*, 02*l*, 04*l*, . . . contain rows of sharp equidistant spots connected by weak streaks and reveal the ≈1.2-nm spacing; whereas the rows 01*l*, 03*l* are continuously and often heavily streaked (Fig. 11). Both sublattices contribute to these rows of reflections since the 0*kl* reflections are common to both reciprocal lattices. A possible explanation for the weak streaks will be given in section 5.2. Similar observations were reported in one of the misfit layer sulfosalts (Franckeite) (*12*).

4. High Resolution Images

4.1 High Resolution Images Along the [001] Zone Axis

High resolution images along the [001] zone axis were obtained for several of the materials. The images consist either of a slightly deformed hexagonal pattern or of a quasi square pattern of bright dots (Figs. 12–14 and 16). Whether one or the other

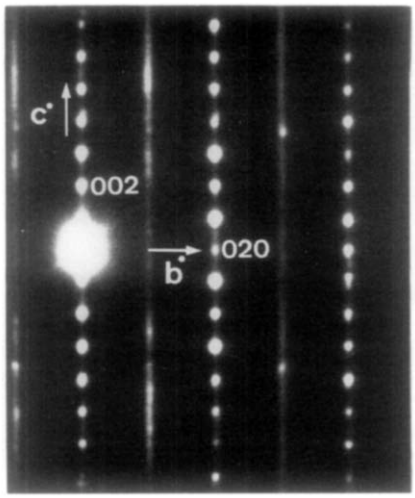

FIG. 11. Electron diffraction pattern along the [100] zone axis in $PbTaS_3$ as observed at the curled edge of a [001] foil and revealing intense streaks along all the rows for which k = odd.

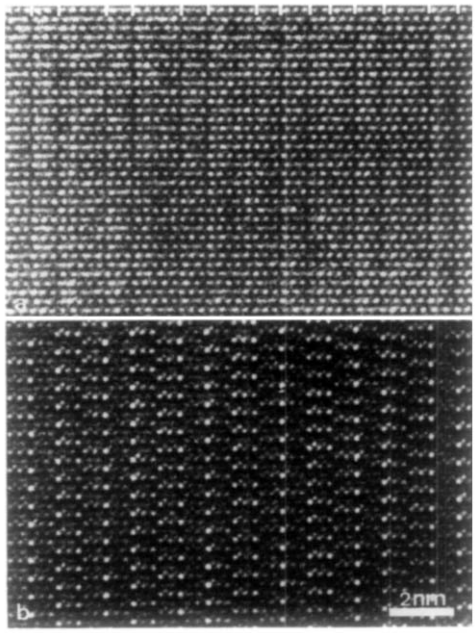

FIG. 13. High resolution image of two adjacent regions with different thicknesses in a [001] foil of $PbTaS_3$ exhibiting an identical sequence of dark (respectively bright) lines along the b-direction. The lines are most probably due to relaxations of Pb atoms into the hollows formed by the S atoms of TaS_2.

pattern will be prominent depends on the diffraction conditions and on the specimen thickness, which also determine the relative intensities of the reflections in the diffraction pattern. If the low order TS_2 spots are the most intense ones in the diffraction pattern the image will prominently exhibit the hexagonal pattern; if on the other hand the MS diffraction spots are the most intense ones the pattern will be prominently square. If both types of spots have comparable intensities the pattern of bright dots will exhibit some intermediate configuration. In spite of their relative simplicity the images reveal the essential features of the complete structure. The most significant feature is the modulation of the intensity of the bright dots along the rows parallel with the misfit a-direction; also the sharpness of the dots tends to vary in the same quasi-periodic way. Depending on the particular compound three or four sharp bright dots alternate with four or three somewhat diffuse less bright dots. In adjacent dot rows

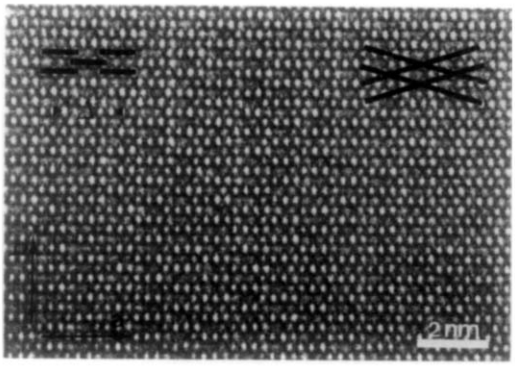

FIG. 12. High resolution image along [001] in $SnNbS_3$ showing a modulated pattern based on a deformed hexagonal dot configuration. The modulation period along the misfit a-direction is $2/\Delta g_1 \approx 6a_2 \approx (7/2)\, a_1$ as was expected from the ratio $a_1/a_2 \approx 12/7$. The directions of the "brightness modulation waves" due to Δg_2 and Δg_3 are indicated.

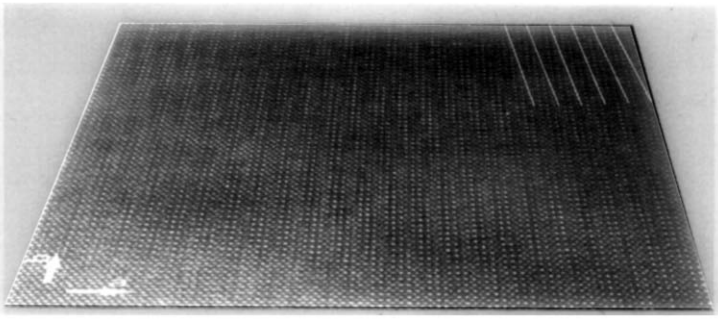

FIG. 14. High-resolution image along [001] in $PbNbS_3$ viewed at grazing incidence along the b-direction revealing "ledging" due to gradual shifts along the misfit a-direction. The new average orientation of the "misfit planes" is indicated.

the modulations are in anti-phase. This gives rise to a quasi-periodic two-dimensional dot pattern which can with good approximation be referred to a centered rectangular unit mesh with dimensions $\Delta \times b$ where $\Delta \approx ma_2 \approx na_1$ (note that $\Delta \approx 2/\Delta g_1$). The numbers m and n for the different compounds can easily be derived as follows:

Consider

$$1/2\ a_1\ (MS) \text{ and } a_2\ (TS_2) \text{ with } a_1 < a_2$$

then

$$a_2 = 1/2\ a_1 + 1/2\ \varepsilon \text{ with } 0 < \varepsilon < a_1.$$

We then also have

$$ka_2 = 1/2\ (ka_1 + k\varepsilon).$$

If $k\varepsilon = a_1$, one obtains

$$(a_1/\varepsilon)a_2 = 1/2\ [a_1/\varepsilon) + 1]a_1$$

and if m is the integer closest to but smaller than

$$a_1/\varepsilon, \text{ i.e., } m = [a_1/e],$$

we obtain

$$ma_2 \leq 1/2\ (m + 1)a_1 \approx \Delta.$$

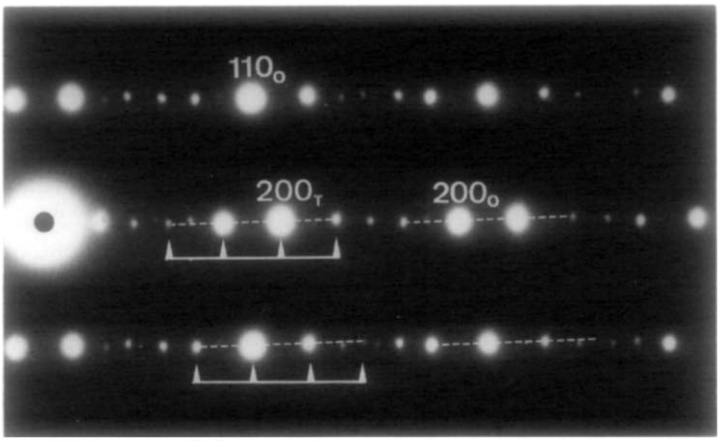

FIG. 15. Electron diffraction pattern in $PbNbS_3$ corresponding with the image of Fig. 14 and revealing an "orientation anomaly": the broken lines connecting satellite sequences with their basic spot enclose a small angle with a^*.

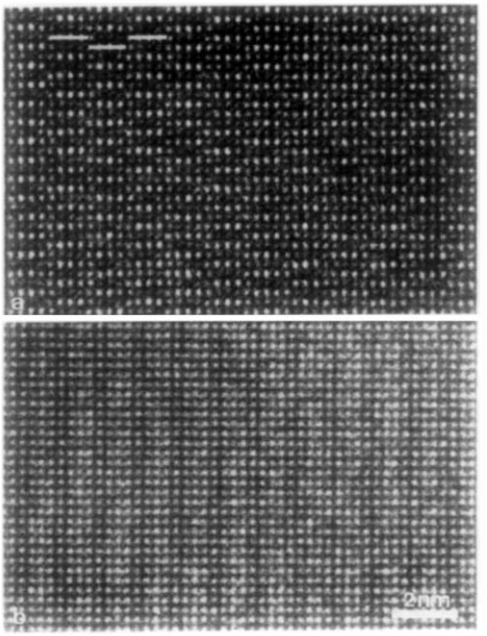

FIG. 16. High resolution images along [001] in different $LaNbS_3$ crystals: (a) The imaged pattern is centered, the modulation period along the misfit a-direction is $\Delta \approx 2/\Delta g_1$ ($\approx 7a_2 \approx 4a_1$). (b) The centering of the pattern is lost, the modulation period along the a-direction is $1/\Delta g_1$. The image pattern in (b) is compatible with systematic $b/2$ shifts of NbS_2 layers, the pattern in (a) is not.

The integers m and $1/2(m + 1)$ or n are then the number of unit cells which lead to the first approximation for the supercell. Applying this to the different compounds leads to the values of m given in Table I. For instance for $LaNbS_3$ one finds $m = 7$ and for $SnNbS_3$, $m = 6$. This means that for the first compound it is a good approximation to choose a supercell containing m (= 7) unit cells of NbS_2 fitting into $1/2$ $(m + 1)$ (= 4) unit cells (eight MS distances!) of LaS. For the second compound the supercell will have to contain $2m$ (= 12) units of NbS_2 fitting approximately onto $m + 1$ (= 7) units of SnS. In the hexagonal image patterns there are m intervals between bright dots in one period Δ; in the square patterns there are $2n$ such intervals since successive columns of the MS structure are not equivalent in space but nevertheless project in the same way on (001). These features can be observed in Figs. 12–14 and 16.

In a number of well-contrasted images dark or bright lines parallel with the b-direction are visible (Figs. 12 and 13). The period of this line pattern is also Δ, but more than one line may occur in each period. In the hexagonal pattern ($PbTaS_3$) of Fig. 13a the dark lines result from the fact that locally the separation of successive bright dots is somewhat larger than the average. There are two prominent dark lines in one period. Between the widest spaced lines there are four (or five) bright dots whereas between the narrower spaced lines there are three (or two) bright dots. In one period Δ there are always seven bright dots, either 4 + 3 or 5 + 2. In the predominantly square pattern ($PbTaS_3$) of Fig. 13b the bright lines are marked by extra bright dots; the period is again Δ and it is subdivided in the same way as the pattern of dark lines. Such dot patterns presumably result from relaxation of the MS structure when juxtaposed onto the TS_2 structure. In both patterns a "phase slip" of the line pattern occurs periodically. This is presumably due to the fact that Δ is not exactly given by $\Delta = ma_2 = na_1$ but that in actual fact ma_2 is slightly different from na_1 and this difference leads to a periodic adjustment of the overlap pattern.

A periodic adjustment can also be assumed from the images where no prominent dark (or bright) lines parallel to b are present; it is then revealed by the fact that the short sequences of extra brights dots are locally (i.e., along a line parallel with a) 1 unit longer or shorter, as for instance in Fig. 12. These features are clearly a direct consequence of the incommensurate nature of the misfit layer structures.

Lines of a similar nature, roughly along the b-direction and formed by extra bright

dots were observed in $PbNbS_3$. In that material the lines sometimes shift sideways by systematic ledging; their average direction then encloses an angle with the *b*-direction (Fig. 14). It supports the view that these lines are some kind of discommensuration lines separating successive strips of best fit, i.e., where the atoms in the *M*S layer fit optimally in the hollows of the TS_2 layers. A small relative shift in the *a*-direction of the two lamellae changes the superposition pattern over the distance between successive hollows in the TS_2 layer and thus changes the positions of the "discommensurations" over the same distance. The (gradual) shift of the bright dot rows over one interrow spacing is clearly visible in Fig. 14. The lines are analogous to the moiré-like fringes observed in $MnSi_{2-x}$; also in this material a systematic relative shift of the silicon helices with respect to the manganese matrix causes an orientation change of the fringes (*16, 17*). A diffraction pattern reveals such systematic "phason" type shifts as orientation anomalies. The pattern corresponding with the crystal area of Fig. 14 is reproduced in Fig. 15. The vector Δg_1 now encloses a small angle with the a^* direction. This small angle can be seen as resulting from a small shear deformation of the lattice of the two lamellae. The orientation anomaly allows to deduce unambiguously in which way the linear sequences of satellites belong together, i.e., which satellites are connected with a given basic reflection; this is indicated by brackets in the pattern of Fig. 15 and it is in agreement with the assumptions made in Section 3.2.

4.2 Computed Images

Image simulations were performed with the structure data derived from X-ray diffraction (*4, 6, 7*). However, in image calculations a strictly periodic model, with $ma_2 = na_1$ exactly satisfied, had to be used; accordingly the atom positions were very slightly adapted. A representative matrix of simulated images for a range of thicknesses and defocus values, computed using the direct space method (*18*), is reproduced in Fig. 17 for the compound $LaNbS_3$. The shift over $b/2$ of subsequent NbS_2 layers as reported from single crystal X-ray data was not taken into account. In spite of this the simulated images clearly have the characteristic features exhibited by most of the observed experimental images.

It is worth noting that the computed image pattern with $\Delta f = -80$ nm and a thickness of 1.15 nm (i.e., 1 unit cell) is square with hardly any brightness modulation, whereas the image pattern for $\Delta f = -80$ nm but at a thickness of 20.7 nm is hexagonal, also without brightness modulation. The transition from one pattern into the other occurs gradually with increasing thickness. The best correspondence with the particular experimental image of $LaNbS_3$ shown in Fig. 16a is found for $t = 6.9$ nm and $\Delta f = -80$ nm. A comparison of the simulated images of Fig. 18 with the model of Fig. 2 shows that for the smaller thicknesses (e.g., $t = 10.6$ nm) and defocus values at or just above Scherzer defocus (≈ -70 nm) the brightest dots correspond with the coincidence sites of atom columns *M*-S and *T*, the brightness being a measure for the degree of straightness of the columns. For the same thicknesses but for defoci just below Scherzer defocus the brighter dots correspond with the centers of the empty trigonal prisms formed by *T* atom columns (Fig. 2). The latter also applies to all Δf values around Scherzer for large thicknesses.

4.3 Intuitive Considerations

The high resolution images can to some extent be understood intuitively. We first note that straight columns of heavy atoms parallel with the incident beam can be imaged as sharp bright (or dark) dots. According to the atomic column approximation (*19*) electrons travelling along such a column are periodically focused and defo-

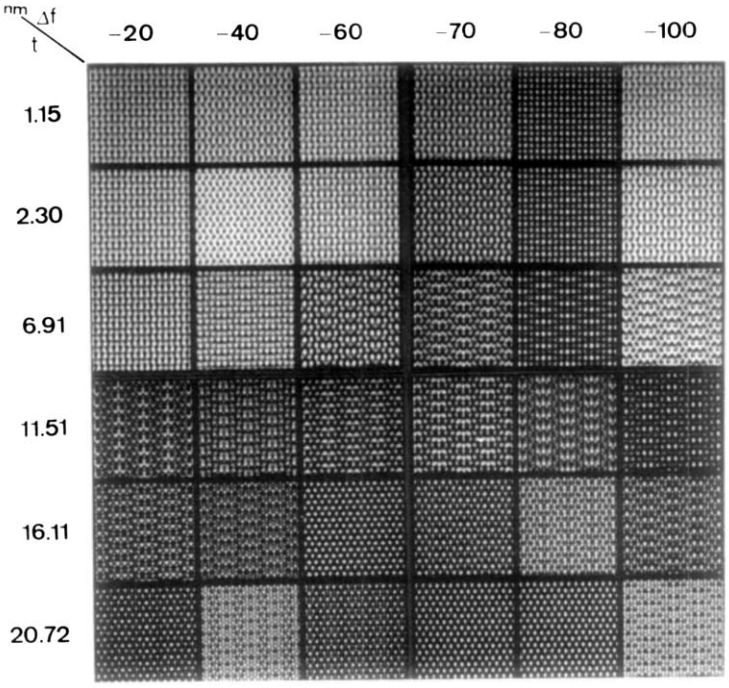

FIG. 17. Matrix of computed high resolution images along [001] in $LaNbS_3$. The $b/2$ shifts of subsequent NbS_2 layers were not taken into account. Instrumental parameters used in the calculations were $V = 200$ kV; $C_s = 1.2$ mm; h.a. beam conv. $= 8 \times 10^{-4}$ rad; def. spread = 7 nm; obj. ap. rad. = 7 nm^{-1}.

cused with a period which depends on the composition (this period is some kind of extinction distance along the length of the column). At the exit surface, i.e., at the bottom of the column, either a relative maximum or a minimum in intensity, i.e., a bright dot or a dark dot, will thus be produced. At constant defocus for a given thickness the M columns may thus produce maxima, i.e., bright dots, while the T columns (or the prismatic tunnels formed by the T columns) may produce bright dots for another thickness.

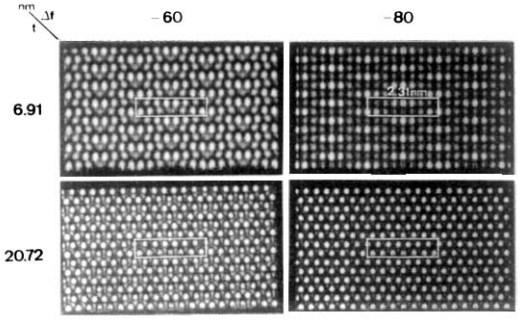

FIG. 18. Computed high resolution images along [001] in $LaNbS_3$ taken from Fig. 17. The repeat unit is outlined. Comparison with the model of Fig. 2 permits the derivation of an imaging code applicable to all MTS_3 compounds.

If the column is not straight but consists of two parts which are laterally shifted, the maximum or the minimum is produced at a position which is intermediate between the projected positions of the two column parts. The final position will be closest to the projected position of that part of the column which contributes most to the final intensity. These considerations follow from image simulations of stacking fault tetrahe-

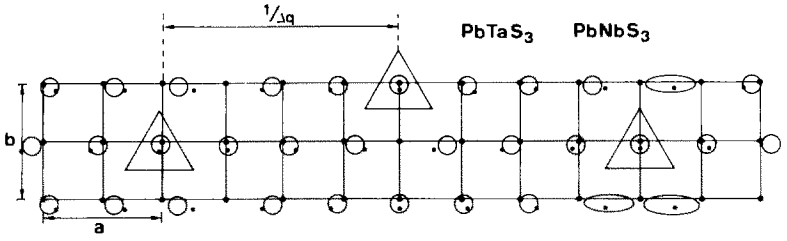

FIG. 19. Projection along [001] of an MTS_3 compound with $a_1/a_2 \approx 7/4$. The circles indicate the intuitively expected dot positions. Under particular conditions a sharp bright dot will be observed only where the separation between atom columns of TS_2 and MS (small and larger black dots) is sufficiently small.

dra in silicon. Silicon columns along [110] intersecting a stacking fault suffer such a lateral shift. They were found to be imaged in a shifted position, the magnitude and sense of the shift depending on the relative lengths of the two column parts (*20*).

In the structures considered here some heavy atom columns in the region of good fit can within good approximation be considered as straight columns; they contain *M*-S and *T* atoms. However, most such columns are zigzag shaped. It is thus to be expected that they will produce a bright dot at an intermediate position and with an intermediate brightness if both parts contribute. We do not consider the sulfur matrix of the TS_2 layers, which does not seem to be imaged under the conditions used.

Using these principles it is possible to qualitatively predict the image for a given structure. If only the *M* atom columns contribute the imaged pattern will be square; if only the *T* atoms contribute it will be hexagonal. However, in general both atom species will contribute; the imaged dots will thus be produced in an intermediate position. This situation is schematically represented in Fig. 19; it is in good qualitative agreement with the observed dot patterns (e.g., Fig. 12).

From a comparison of the simulated images with the model it is confirmed that the brightest sharp dots indeed correspond with well-defined (nearly) straight columns under the appropriate imaging conditions.

5. Discussion

5.1 Stacking Disorder

The present study has revealed a number of features which are apparently in contradiction with the X-ray diffraction results (*4*, *6–8*).

The [001] electron diffraction patterns exhibit $hh0_T$ reflections which cannot be explained by double diffraction but which on the contrary are strong enough to excite satellite spots at $hh0_T \pm \Delta g_i$ ($i = 1$ to 3). The intensity of these $hh0_T$ reflections is rather low and somewhat variable but they are never completely absent. Such reflections should not appear if the MS sublattice is strictly face-centered; they are compatible with *C*-centering of this sublattice, however.

In the same zone also the TS_2 subpattern exhibits $hh0_o$ reflections which should normally be absent in a face-centered lattice. The spots cannot be explained by double diffraction but on the contrary again excite reflections at $hh0_o \pm \Delta g_i$. Their presence is compatible with *C*-centering of the TS_2 sublattice.

Very occasionally spots $0k0$ (k = odd) are observed in the [001] patterns. These spots

are in contradiction not only with face-centering but with *C*-centering as well.

In the [100] zone pattern, which contains the common $0kl$ reflections, only reflections with k = even should be present if the lattice is *C*-centered. However, at the rows k = odd one observes streaks (occasionally with sharp reinforcements) (Fig. 11) indicating that k = odd reflections are present but that one-dimensional disorder along the *c*-axis causes their degeneration into streaks. This leads to the assumption that the exact centering of individual layers might be lost due to atom relaxations associated with the mutual modulation of the substructures.

In general the $hk0$ reflections with h = odd, k = even and those with h = even, k = odd are absent showing that the *C*-centering is still preserved in projection and that the assumed breaking of the *C*-centering will mainly have to be attributed to displacements out of the layer planes, i.e., along the *c*-direction. The vector relating motifs at the corner and at the *C*-center can then be written as $1/2\ [1, 1, \varepsilon]$ with respect to a unit cell a_1 (or a_2) $\times\ b \times 2c$, where ε is a rudimentary representation of the symmetry breaking relaxation.

On the basis of the arguments of section 2.2 successive layers of the same type are assumed to either be stacked vertically one above the other or to be shifted over $b/2$.

Formally the lattice part of the structure factor can then be written as

(a) in the case of "vertical" stacking (no shift)

$$\{1 + \exp \pi i(h + k + l\varepsilon)\}\{1 + \exp \pi il\} \tag{1}$$

(b) in the case of pseudo-face-centered stacking (systematic shift)

$$\{1 + \exp \pi i(h + k + l\varepsilon)\}\{1 + \exp \pi i(k + l)\}. \tag{2}$$

In case (a) the criterion for $hk0$ reflections to be present is $h + k$ = even, allowing for $hh0$ reflections as observed in [001] zone patterns. For the $0kl$ reflections Eq. (1) reduces to

(i) $(1 + \exp \pi i\, l\varepsilon)\ (1 + \exp \pi i\, l)$ for k = even;

i.e., only reflections with l = even and $l\varepsilon \neq$ odd integer are allowed. A maximum is expected for l = even, $l\varepsilon$ = even integer.

(ii) $(1 - \exp \pi i\, l\varepsilon)\ (1 + \exp \pi i\, l)$ for k = odd;

i.e., only reflections with l = even ($l \neq 0$) and $l\varepsilon \neq$ even integer are allowed. A maxi-

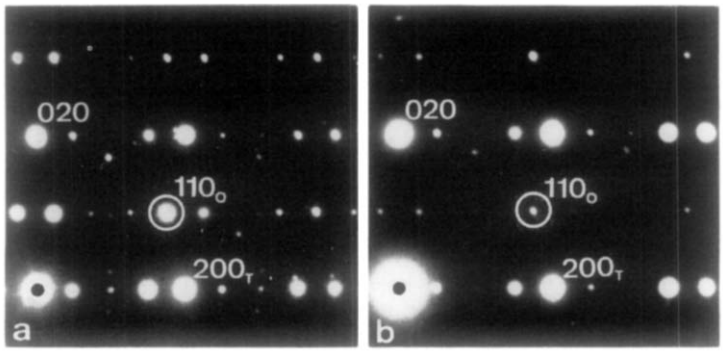

FIG. 20. Electron diffraction patterns along [001] in different $LaNbS_3$ crystals. The corresponding images are shown in Fig. 16. The high relative intensity of the 110_o spot in (a) is not compatible with a systematic $b/2$ shift of NbS_2 layers. The weakened 110_o reflection in (b) can be attributed to the presence of such $b/2$ shifts.

mum is expected for l = even, $l\varepsilon$ = odd integer.

In case (b) $hk0$ reflections are only allowed if h and k are both even, i.e., $hh0$ reflections with h = odd should be extinct. However, reflections of the latter type are present in [001] zone patterns which thus contradict face-centering. For the $0kl$ reflections Eq. (2) reduces to $(1 + \exp \pi i\, l\varepsilon)$ $(1 + \exp \pi i\, l)$ for k = even;
i.e., only reflections with l = even and $l\varepsilon \neq$ odd integer are allowed.
$(1 - \exp \pi i\, l\varepsilon)$ $(1 - \exp \pi i\, l)$ for k = odd;
i.e., only reflections with l = odd and $l\varepsilon \neq$ even integer are allowed.

In the case of a disordered stacking along c with fault vector R = 1/2 [010] the reflections for which $g \cdot R \neq$ integer will become diffuse, i.e., the c^* rows for which k = odd will become streaked, which is in agreement with the observations in the [100] zone patterns. Since localized intensity is present along the c^* rows with k = odd in the case of vertical stacking as well as in the case of "shifted" stacking it is concluded that the actual stacking of lamellae of the same type must be a disordered stacking, i.e., certain lamellae will be stacked in the pseudo-face-centered manner but the majority will be stacked in the vertical manner.

In the rows k = even only sharp reflections at l = even are observed as predicted.

5.2 The b/2 Shift

For most compounds (except $SnTS_3$) X-ray diffraction finds a doubling of the c-parameter due to relative shifts over $b/2$ of successive TS_2 layers (or of both MS and TS_2 layers) (*8*). The shifts account for the face-centering of the corresponding unit as deduced from the systematic extinction of all reflections with mixed indices (not all odd or all even).

Due to the geometry itself of the MS slabs relative displacements over $b/2$ of successive MS layers will not visibly influence the high resolution images; here we will therefore concentrate on the TS_2 layers.

In selected area electron diffraction patterns along the [001] zone axis the face-centering, i.e., the systematic shift of subsequent TS_2 layers, will give rise to near extinction of all $hk0_o$ reflections for which both h and k are not even (Section 5.1). As

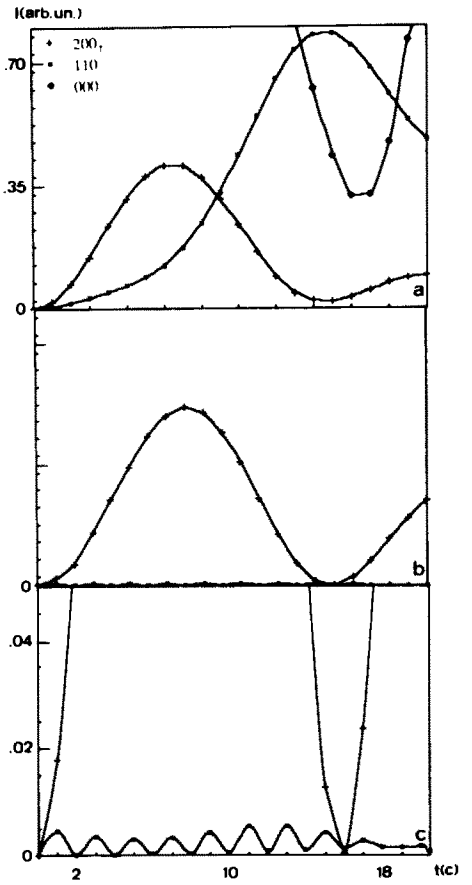

FIG. 21. Plot of calculated dynamical intensity I (arbitrary units) versus foil thickness t (in c-units; c = 1.15 nm) for the 000, 200_T, and 110_o reflections of $LaNbS_3$ in the case of (a) no relative $b/2$ shift of successive NbS_2 layers; (b) relative $b/2$ shift; (c) same as (b) but I-axis expanded (16 times) in order to show the influence of an odd number of NbS_2 layers on the diffracted intensity.

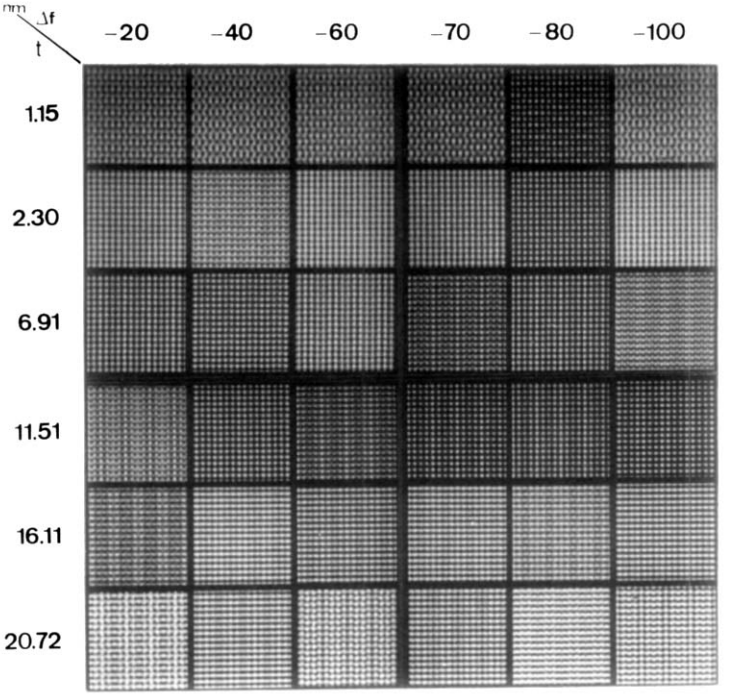

FIG. 22. Matrix of computed high resolution images along [001] in $LaNbS_3$. The $b/2$ shifts of subsequent NbS_2 layers as found from X-ray diffraction were taken into account. The instrumental parameters are as in the legend to Fig. 17.

a result of the weakening of the 110_o spot Δg_1 will remain as the only prominent difference vector. This is indeed observed in some cases (e.g., Fig. 20b). Total extinction will never occur since in general (part of) the selected foil region will contain an odd number of TS_2 slabs, thus breaking exact face-centering. Some residual intensity could also be due to to local disorder on the T-lattice as is in fact suggested in (*6*) for $PbNbS_3$. In Fig. 21 the dynamical intensities of the 110_o and 200_T reflections in the case of "no shift" (Fig. 21a) and "shift" (Figs. 21b and 21c) are plotted as a function of foil thickness. It is obvious that even when the foil comprises an odd number of shifted TS_2 layers the intensity of the 110_o reflection is much lower than that of the 200_T reflection (except for a small thickness interval around 17 nm).

One can state that observing an intensity for the 110_o reflection comparable with or larger than that of the 200_T reflection over a range of thicknesses is not compatible with the relative $b/2$ shift of successive TS_2 layers. However, diffraction patterns with the latter characteristics are frequently observed in all MTS_3 compounds.

For the matrix of computed high resolution images along the [001] zone axis shown in Fig. 22 the $b/2$ shift was included. These simulated images are to be compared with the matrix of Fig. 17 where no displacements were taken into account. Note that for $t = 1.15$ nm the computed micrographs are identical for both cases (Figs. 17 and 22) as they should be since the foil comprises only one slab of each type and consequently a relative shift cannot play a part yet. Due to the relative displacements of

subsequent TS_2 layers over $b/2$ the centering of the supercell is lost. The atom column separation in the TS_2 part cannot be resolved any more and the computed images reveal a predominantly square pattern of dots with only a weak modulation along the misfit a-direction due to the only prominent difference vector Δg_1. An example of such an image is shown in Fig. 16b; it corresponds with the electron diffraction pattern of Fig. 20b. Obviously, high resolution images revealing a centered supercell configuration or a modulated hexagonal configuration of dots are not compatible with the $b/2$ shift. Nevertheless, images with the latter characteristics are more frequently observed.

It is concluded that although the systematic $b/2$ shifts of successive TS_2 layers as found from X-ray diffraction do occur in certain crystals of all (except $SnTS_3$) compounds, they are not a general characteristic. However, it is most likely that such displacements occur nonsystematically in most crystal foils as is also strongly suggested by the electron diffraction data discussed in Section 5.1.

Acknowledgments

The authors thank Dr. G. A. Wiegers and his coworkers (Rijksuniversiteit Groningen, The Netherlands) for fruitful discussions and for kindly providing single crystals and preprints of their work.

References

1. G. A. WIEGERS, R. J. HAANGE, AND J. L. DE BOER, *Mater. Res. Bull.* **23,** 1551 (1988).
2. L. GUEMAS, P. RABU, A. MEERSCHAUT, AND J. ROUXEL, *Mater. Res. Bull.* **23,** 1061 (1988).
3. A. MEERSCHAUT, P. RABU, AND J. ROUXEL, *J. Solid State Chem.* **78,** 35 (1989).
4. A. MEETSMA, G. A. WIEGERS, R. J. HAANGE, AND J. L. DE BOER, *Acta Crystallogr. A* **45,** 285 (1989).
5. S. KUYPERS, G. VAN TENDELOO, J. VAN LANDUYT, AND S. AMELINCKX, *Acta Crystallogr. A* **45,** 291 (1989).
6. G. A. WIEGERS, A. MEETSMA, R. J. HAANGE, S. VAN SMAALEN, J. L. DE BOER, A. MEERSCHAUT, P. RABU, AND J. ROUXEL, *Acta Crystallogr.*, in press.
7. J. WULFF, A. MEETSMA, S. VAN SMAALEN, R. J. HAANGE, J. L. DE BOER, AND G. A. WIEGERS, *J. Solid State Chem.* **86,** 118 (1990).
8. G. A. WIEGERS, A. MEETSMA, S. VAN SMAALEN, R. J. HAANGE, J. WULFF, T. ZEINSTRA, J. L. DE BOER, S. KUYPERS, G. VAN TENDELOO, J. VAN LANDUYT, S. AMELINCKX, A. MEERSCHAUT, P. RABU, AND J. ROUXEL, *Solid State Comm.* **70,** 409 (1989).
9. E. MACKOVICKY AND B. G. HYDE, *Struct. Bond.* **46,** 101 (1981).
10. L. OTERO-DIAZ, J. D. FITZGERALD, T. B. WILLIAMS, AND B. G. HYDE, *Acta Crystallogr. B* **41,** 405 (1985).
11. T. B. WILLIAMS AND B. G. HYDE, *Acta Crystallogr. B* **44,** 467 (1988).
12. T. B. WILLIAMS AND B. G. HYDE, *Phys. Chem. Miner.* **15,** 521 (1988).
13. T. B. WILLIAMS AND A. PRING, *Amer. Mineral.* **73,** 1426 (1988).
14. A. JANNER AND T. JANSSEN, *Acta Crystallogr. A* **36,** 408 (1980).
15. S. VAN SMAALEN, *Phys. Rev. Lett.*, in press.
16. R. DE RIDDER, G. VAN TENDELOO, AND S. AMELINCKX, *Phys. Status Solidi A* **33,** 383 (1976).
17. H. Q. YE AND S. AMELINCKX, *J. Solid State Chem.* **61,** 8 (1986).
18. W. COENE AND D. VAN DYCK, *Ultramicroscopy* **15,** 41 (1984).
19. D. VAN DYCK, J. DANCKAERT, W. COENE, E. SELDERSLAGHS, D. BRODDIN, J. VAN LANDUYT, AND S. AMELINCKX, "Computer Simulation of E. M. Diffraction & Images" (W. Krakow and M. O'Keefe, Eds.), (1989), 107–134.
20. W. COENE, H. BENDER, AND S. AMELINCKX, *Philos. Mag., A* **52,** 369 (1985).